Interface resistance of biomolecular condensates

Yaojun Zhang,[1,2,3,*] Andrew G.T. Pyo,[4] Yoyo Jiang,[2] Clifford P. Brangwynne,[5,6] Howard A. Stone,[7] and Ned S. Wingreen[8,9,*]

[1] *Center for the Physics of Biological Function, Princeton University, Princeton, NJ, USA*
[2] *Department of Physics and Astronomy, Johns Hopkins University, Baltimore, MD, USA*
[3] *Department of Biophysics, Johns Hopkins University, Baltimore, MD, USA*
[4] *Department of Physics, Princeton University, Princeton, NJ, USA*
[5] *Department of Chemical and Biological Engineering, Princeton University, Princeton, NJ, USA*
[6] *Howard Hughes Medical Institute, Chevy Chase, MD, USA*
[7] *Department of Mechanical and Aerospace Engineering, Princeton University, Princeton, NJ, USA*
[8] *Department of Molecular Biology, Princeton University, Princeton, NJ, USA*
[9] *Lewis-Sigler Institute for Integrative Genomics, Princeton University, Princeton, NJ, USA*

I. ABSTRACT

A hallmark of biomolecular condensates formed via liquid-liquid phase separation is the dynamic exchange of condensate components with the surroundings. Such material exchange can be key to condensate function, as the rate of component exchange can impact biochemical reaction rates in the condensates, the speed of response of condensates to a changing environment, and their number and sizes. How is this exchange rate controlled? Intuitively, this rate can be limited by the flux of materials from the dilute phase or by the speed of mixing inside the dense phase. Surprisingly, recent experiments suggest that this rate can also be limited by the dynamics of molecules at the droplet interface, implying the existence of an "interface resistance". Here, we combined theory and simulation to show that an interface resistance can arise when incident molecules contact the interface without entering the dense phase. We find that such "bouncing" occurs for incident molecules that are capable of self-collapse into a non-sticking conformation. Our work highlights the underappreciated role of interface resistance in condensate exchange dynamics, with implications for natural and synthetic systems.

II. MAIN

The interior of cells is organized in both space and time by biomolecular condensates, which form and dissolve as needed [1, 2]. These condensates play key roles in processes ranging from transcription to translation, metabolism, signaling, and more [3–6]. The complex interactions among their components endow condensates with distinct physical properties, including low surface tension, viscoelasticity, aging, etc. These distinct properties are crucial to the ability of condensates to carry out their unique biological functions. Here, we focus on one important physical property of condensates – the rate of exchange of material between condensed and dilute phases. This rate of exchange can impact biochemical processes taking place in condensates by limiting the escape of completed products, such as ribosomes produced in nucleoli [7], or limiting the availability of component or regulatory molecules (e.g. snoRNAs and ribosomal proteins entering nucleoli, or mRNAs entering P bodies or stress granules) . The rate of exchange can also control the dynamical response of condensates to a changing environment, and, as exchange between dense and dilute phase is central to coarsening via Ostwald ripening, it can regulate the number, size, and location of condensates within the cell.

The material exchange between a condensate and the surrounding dilute phase can be probed by FRAP-type experiments in which, e.g., fluorescence is locally bleached and recovery as a function of time recorded (Fig. 1a,b). Theoretically, the time evolution of the concentration profile $c(r,t)$ of the molecules initially located in a spherical condensate of radius R (bleached population) can be described by the following continuum diffusion equations [8]:

$$\begin{aligned}\frac{\partial}{\partial t}c(r,t) &= D_{\rm den}\left(\frac{\partial^2}{\partial r^2}+\frac{2}{r}\frac{\partial}{\partial r}\right)c(r,t), \quad r<R;\\ \frac{\partial}{\partial t}c(r,t) &= D_{\rm dil}\left(\frac{\partial^2}{\partial r^2}+\frac{2}{r}\frac{\partial}{\partial r}\right)c(r,t), \quad r>R, \end{aligned} \tag{1}$$

with the initial condition:

$$c(r,0)=\begin{cases} c_{\rm den}, & r<R;\\ 0, & r>R,\end{cases} \tag{2}$$

and boundary conditions:

$$\begin{aligned}\frac{\partial}{\partial r}c(r,t)|_{r=0} &= c(+\infty,t)=0;\\ -D_{\rm den}\frac{\partial}{\partial r}c(r,t)|_{r=R_-} &= -D_{\rm dil}\frac{\partial}{\partial r}c(r,t)|_{r=R_+}\\ &= \kappa\left[c(R_-,t)-\frac{c_{\rm den}}{c_{\rm dil}}c(R_+,t)\right],\end{aligned} \tag{3}$$

where $D_{\rm den}$ and $D_{\rm dil}$ are the diffusion coefficients of molecules in the dense and dilute phases, and $c_{\rm den}$ and $c_{\rm dil}$

* Email: yaojunz@jhu.edu; wingreen@princeton.edu

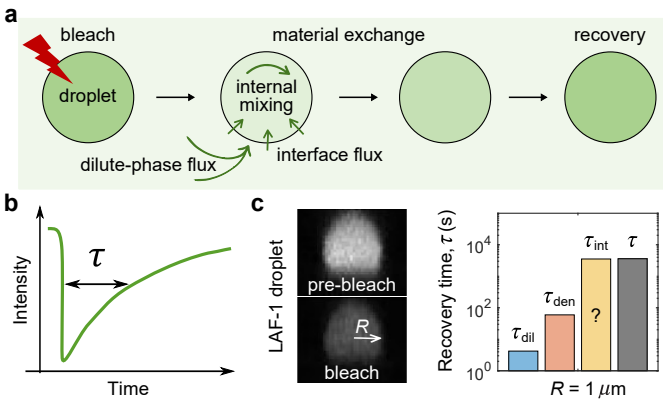

FIG. 1. **FRAP experiments on droplets.** **a**, Schematic of FRAP experiment in which an entire droplet is photobleached and the recovery of fluorescence is recorded. Material exchange between the condensate and the surrounding dilute phase can be limited by the flux of unbleached molecules coming from the dilute phase, the speed of internal mixing in the dense phase, or the flux passing through the interface. **b**, The recovery time τ is defined as the time required for fluorescence to return 63% (i.e. $1-1/e$) of the way back to its original level. **c**, Experimental data from Ref. [8] in which a LAF-1 droplet of radius $R = 1\,\mu$m recovers from photobleaching. Images before bleaching (top left) and immediately after bleaching of the entire droplet region (bottom left). (Right) Expected recovery time $\tau_{\rm dil} = c_{\rm den}R^2/(3c_{\rm dil}D_{\rm dil}) = 4\,$s and $\tau_{\rm den} = R^2/(\pi^2 D_{\rm den}) = 60\,$s if the slowest recovery process is the flux from the dilute phase or diffusion within the droplet, respectively, where $D_{\rm den} = 0.0017\,\mu{\rm m}^2/{\rm s}$, $D_{\rm dil} = 94\,\mu{\rm m}^2/{\rm s}$, and $c_{\rm den}/c_{\rm dil} = 1190$. While the timescale associated with interface resistance $\tau_{\rm int}$ is unknown, the measured recovery time $\tau \sim 1\,$hour is much longer than $\tau_{\rm dil}$ and $\tau_{\rm den}$, suggesting the recovery is limited by flux through the interface.

are the equilibrium concentrations in the dense and dilute phases. The second boundary condition corresponds to flux balance at the interface of the condensate. Specifically, the flux exiting the dense phase (left) equals the flux entering the dilute phase (middle) and also equals the flux passing through the interface (right). κ is a transfer coefficient that governs the magnitude of the net flux, which is nonzero when the ratio of the concentrations on the two sides of the interface deviates from its equilibrium value. We term κ the interface conductance, the inverse of interface resistance.

For the model described by equations (1)-(3), the fraction of molecules in the condensate which are unbleached at time t is

$$f(t) = 1 - \frac{\int_0^R 4\pi r^2 c(r,t)dr}{\int_0^R 4\pi r^2 c_{\rm den} dr}. \tag{4}$$

Clearly, how quickly $f(t)$ recovers from 0 to 1 quantifies the timescale of material exchange between the condensate and the surrounding dilute phase. The authors of [8] derived an exact solution for $f(t)$ in an integral form using Laplace transforms. However, it is not directly apparent from the integral expression what physics governs the timescale of fluorescence recovery. To obtain a more intuitive result, we note that diffusion of biomolecules in the dilute phase is typically much faster than diffusion in the dense phase, with measured $D_{\rm dil}/D_{\rm den}$ in the range of $10^2 - 10^5$ [8, 9]. We therefore employed the exact solution to derive an approximate solution in the parameter regime $D_{\rm dil} \gg D_{\rm den}$:

$$f(t) \approx 1 - \exp\left(-t/\tau\right), \tag{5}$$

where the timescale of fluorescence recovery is set by:

$$\tau = \frac{R^2}{\pi^2 D_{\rm den}} + \frac{c_{\rm den}R^2}{3c_{\rm dil}D_{\rm dil}} + \frac{R}{3\kappa}. \tag{6}$$

Equation (6) conveys a clear physical picture of what controls the timescale of condensate material exchange. First, for large condensates and slow internal diffusion, exchange is limited by the rate of mixing within the condensate, so that $\tau \simeq R^2/(\pi^2 D_{\rm den})$. Second, if diffusion in the dilute phase is not fast enough, or the concentration in the dilute phase is very low, then $\tau \simeq c_{\rm den}R^2/(3c_{\rm dil}D_{\rm dil})$, which is the time required to replace all molecules in the condensate if molecules incident from the dilute phase are immediately absorbed (see Supplementary note). Finally, if the interface conductance κ is very small, the interfacial flux can be rate limiting for exchange, yielding $\tau \simeq R/(3\kappa)$.

What determines the magnitude of the interface conductance κ? From a theoretical perspective, transitions between dense and dilute phases have been modeled both by considering single-molecule trajectories [10] and from the perspective of continuum theory [11]. However, for any particular systems, the magnitude of the interface conductance depends on microscopic features of the biomolecules which may not be captured by Flory-Huggins and Cahn-Hilliard-type mean-field theories. Indeed, if we start with the continuum approach in [11], where the concentration of bleached components $c(\mathbf{r},t)$ is governed by

$$\frac{\partial}{\partial t}c(\mathbf{r},t) = \nabla\cdot\left\{D[c_{\rm eq}(\mathbf{r})]\left[\nabla c(\mathbf{r},t) - c(\mathbf{r},t)\frac{\nabla c_{\rm eq}(\mathbf{r})}{c_{\rm eq}(\mathbf{r})}\right]\right\}, \tag{7}$$

with $c_{\rm eq}(\mathbf{r})$ the equilibrium concentration profile and $D[c_{\rm eq}(\mathbf{r})]$ the diffusion coefficient which depends on the local equilibrium concentration, one can obtain an expression for κ (see Supplementary note):

$$\kappa^{-1} = \int \frac{c_{\rm den}}{c_{\rm eq}(r)D(r)}dr, \tag{8}$$

where the integral is over the interface region. We would then conclude $\kappa^{-1} < \delta/D_{\rm den} + \delta c_{\rm den}/(c_{\rm dil}D_{\rm dil})$, where δ is the width of the interface. As the interface is typically narrow, this inequality would imply that in practice the interface term in equation (6) would always be smaller than the sum of the other two terms, and thus could be neglected.

However, a recent FRAP experiment on LAF-1 protein droplets [8] contradicts the above mean-field result. In the experiment, a micron-sized LAF-1 droplet

($R = 1\,\mu$m) was bleached and fluorescence recovery measured as a function of time (Fig. 1c). It was observed that recovery of that droplet occurs on a timescale of ~ 1 hour. Given the measured parameters of the system, one can estimate the recovery time in the mean-field approach to be $\tau = R^2/(\pi^2 D_{\rm den}) + c_{\rm den}R^2/(3c_{\rm dil}D_{\rm dil}) = 64\,$s, much shorter than the measured recovery time. A large interface resistance was proposed as a possible explanation for this discrepancy [8]. What could be the underlying mechanism giving rise to such an unexpectedly large interface resistance? Or, more generally, how does interface resistance depend on the microscopic features of phase-separating molecules?

To address these questions, we employed a "sticker and spacer" model [12, 13], which has become a standard tool for the study of phase-separating biopolymers. The "stickers" represent residues or larger domains that are capable of forming bonds in a one-to-one saturable manner, while the "spacers" connect the stickers to form polymers. Specifically, we simulated polymers consisting of type A and type B stickers connected by implicit "spacers" in the form of stretchable bonds [14] (Fig. 2a):

$$U_{\rm b}(r) = -\frac{1}{2}KR_0^2 \ln\left[1-(r/R_0)^2\right], \quad r < R_0, \qquad (9)$$

where r is the distance between two stickers. One-to-one heterotypic bonds between A and B are implemented via an attractive potential:

$$U_{\rm a}(r) = -\frac{1}{2}U_0\left(1+\cos\frac{\pi r}{r_0}\right), \quad r < r_0, \qquad (10)$$

while stickers of the same type interact through a repulsive potential to prevent many-to-one binding:

$$U_{\rm r}(r) = 4\epsilon\left[(\sigma/r)^{12} - (\sigma/r)^6\right] + \epsilon, \quad r \le r_{\rm c}. \qquad (11)$$

We take $K = 0.15\,k_{\rm B}T/{\rm nm}^2$, $R_0 = 10\,$nm, $U_0 = 14\,k_{\rm B}T$, $r_0 = 1\,$nm, $\epsilon = 1\,k_{\rm B}T$, $\sigma = 2\,$nm, and $r_{\rm c} = 1.12\sigma$ in all simulations.

For each of the five sequences shown in Fig. 2a, we simulated 1000 polymers in a $500\,{\rm nm} \times 50\,{\rm nm} \times 50\,{\rm nm}$ box with periodic boundary conditions using Langevin dynamics (see Supplementary note for details). Simulations were performed using LAMMPS [15, 16]. Figure 2b shows a snapshot of coexisting dense and dilute phases after equilibration of the A6B6 polymers (6 A stickers followed by 6 B stickers), while Fig. 2c shows the time-averaged profile of the total sticker density. The five different polymer sequences we simulated were chosen to yield a range of dilute- and dense-phase sticker concentrations (Fig. 2d) as well as a range of dilute- and dense-phase diffusion coefficients (Fig. 2e). As found previously [17], polymers with long blocks of stickers of the same type have low dilute-phase concentrations. This follows because it is entropically unfavorable for these polymers to form self-bonds, which favors the dense phase where these polymers can readily form trans-bonds. These long-block polymers also have low dense-phase diffusion coefficients because of their large number of trans-bonds,

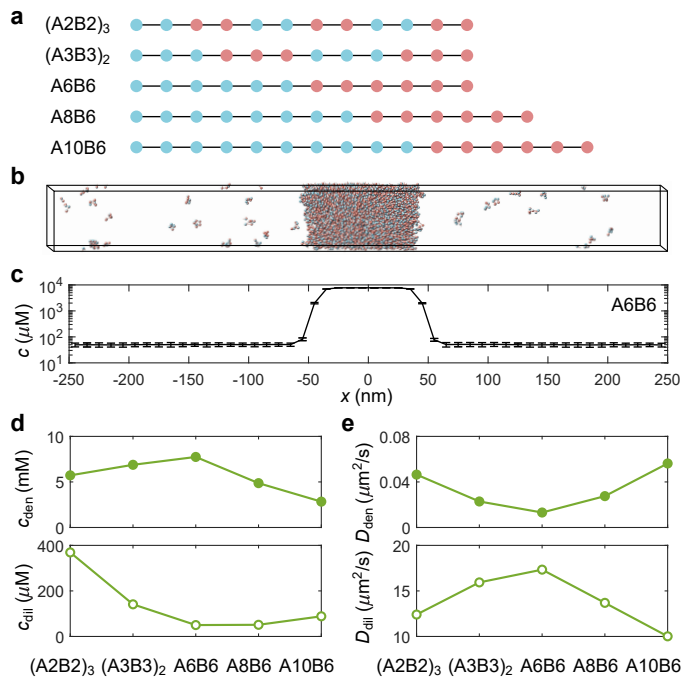

FIG. 2. **Coarse-grained molecular-dynamics simulations of multivalent phase-separating polymers.** **a**, Each polymer is composed of monomers ("stickers") of type A (blue) or B (red), and modeled as a linear chain of spherical particles each with a diameter of 2 nm, connected by stretchable bonds with an equilibrium length of 3.9 nm. Stickers of different types have an attractive interaction, while stickers of the same type interact repulsively, ensuring one-to-one binding between the A and B stickers. **b**, Snapshot of a simulation of 1000 A6B6 polymers in a 500 nm × 50 nm × 50 nm box with periodic boundary conditions. The system undergoes phase separation into a dense phase (middle region) and a dilute phase (two sides), driven by the one-to-one A-B bonds. **c**, Sticker concentration profile for the simulation in (**b**) with the center of the dense phase aligned at $x = 0$ and averaged over time and over ten simulation repeats (see Supplementary note). **d**, Average total sticker concentrations in the dense (top) and dilute (bottom) phases from simulations of the five types of polymers shown in (**a**). **e**, Polymer diffusion coefficients in the dense (top) and dilute (bottom) phases from the same simulations in (**d**). All simulations were performed and snapshots were obtained using LAMMPS [15, 16].

which need to be repeatedly broken for the polymers to diffuse.

Having determined the concentrations and diffusion coefficients in the dense and dilute phases, we are now in a position to extract the values of interface conductance from simulations. Figure 3a depicts a simple protocol that allows us to infer κ by comparing simulations to the 1D, slab-geometry version of equations (1)-(6) (see Supplementary note for details): (i) All polymers in the dilute phase are initially considered "labeled", (ii) any labeled polymer that forms an A-B bond with a polymer in the dense phase becomes permanently unlabeled, (iii) the remaining fraction of labeled dilute phase polymers is

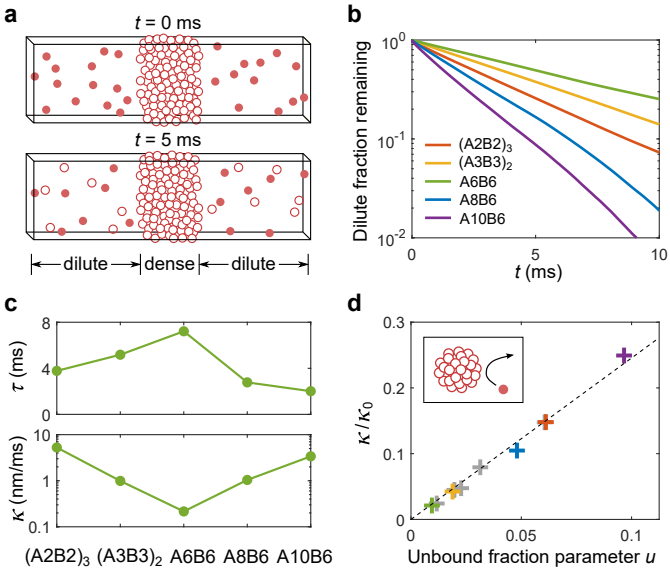

FIG. 3. **Determination of interface conductance from simulations.** **a**, Illustration of simulation protocol: At $t = 0$ only polymers in the dilute phase are "labeled" (solid balls), any polymer that enters the dense phase becomes permanently "unlabeled" (hollow balls). **b**, Fraction of labeled polymers in the dilute phase as a function of time for simulations of the five types of polymers shown in Fig. 2a. **c**, Decay time of labeled polymers from exponential fits to curves in (**b**) (top), and corresponding calculated values of interface conductance κ (bottom). **d**, For all simulated polymers, interface conductance scaled by κ_0 (equation (12)) is approximately a linear function of a parameter u which reflects the fraction of unbound stickers in the dense and dilute phases. Inset illustration: Polymers in the dilute phase with few or no unbound stickers may "bounce" off the dense phase, which contributes to the interface resistance.

fit to exponential decay (Fig. 3b), and (iv) the resulting decay time constant τ is used together with the known dense and dilute phase parameters to infer κ. As shown in Fig. 3c, the resulting values of κ span more than an order of magnitude for our selected polymer sequences, despite the fact that all five can in principle form the same number (6) of self-bonds. What gives rise to the very different values of κ?

To address this question, we first consider the predicted interface conductance κ_0 if polymers incident from the dilute phase simply move through the interface region with a local diffusion coefficient that crosses over from $D_{\rm dil}$ to $D_{\rm den}$. Then according to equation (8) (see Supplementary note)

$$\kappa_0 = \frac{D_{\rm den}}{\delta}\frac{1}{1+(c_{\rm den}/c_{\rm dil})(D_{\rm den}/D_{\rm dil})}. \qquad (12)$$

However, as shown in Fig. 3d, the actual values of κ in our simulations can be a factor of ~ 50 smaller than κ_0. This reduction can be traced to a "bouncing" effect as shown schematically in the inset to Fig. 3d: molecules incident from the dilute phase may fail to form bonds with the dense phase, effectively "bouncing" off of the condensate. The differing extent of this bouncing effect for the five sequences we studied reflects differences in their numbers of free stickers in their dilute phase conformations. The fewer such available stickers, the fewer ways to bond with polymers at the surface of the dense phase, and thus the more likely the incident polymer is to bounce. In support of this picture, we find that all our simulation results for κ/κ_0 collapse as a linear function of a lumped parameter

$$u = \frac{2\pi\sigma\delta^2 c_{\rm den}}{2+s+s^{-1}}(f_{\rm dilA}f_{\rm denB} + f_{\rm dilB}f_{\rm denA}), \qquad (13)$$

which expresses the availability of free stickers (see Supplementary note), where s is the global stoichiometry (i.e. $c_{\rm A}/c_{\rm B}$), $f_{\rm dilA/dilB}$ and $f_{\rm denA/denB}$ are the fractions of bound A/B monomers in the dilute and dense phases, and δ is the width of the interface, all determined from simulations.

In addition to comparing sequences with different block lengths, $(A2B2)_3$, $(A3B3)_2$, A6B6, we included two sequences, A8B6 and A10B6, with unequal sticker stoichiometry. We found that the extra A stickers had only a modest effect on dense and dilute phase properties, but substantially increased the interface conductance κ compared to the most-closely related equal-stoichiometry case A6B6. Intuitively, the excess As in both dense and dilute phases of A8B6 and A10B6 provide a pool of available stickers for any unbound B to bind to. By contrast, at equal stoichiometry both free As and free Bs are rare, which maximizes the bouncing effect. This reduction in potential binding partners at equal stoichiometry has been also observed both experimentally [18] and theoretically [19] to cause an anomalous slowing of diffusion within condensates at equal stoichiometry.

Under what circumstances is interface resistance experimentally measurable? If there were no bouncing effect, i.e. if $\kappa \simeq \kappa_0$, then in practice interface resistance would never dominate the recovery time in FRAP-type experiments. Recovery would be limited either by diffusion in the dense phase or diffusion in the dilute phase, which would also make it very difficult to measure κ. However, as shown in Fig. 3, the bouncing effect can reduce κ significantly. For such systems, the interface conductance can be inferred quantitatively by fitting FRAP recovery curves as in Taylor et al. [8] or simply using equations (5)-(6), provided the dense phase and dilute phase concentrations and diffusion coefficients are known. Even without knowing these parameters, one may still be able to infer the presence of a large interface resistance by observing the pattern of fluorescence recovery in droplets of different sizes: According to equation (6) the recovery time associated with interface resistance increases linearly with radius R while the other terms increase as R^2 (Fig. 4a). Therefore, one expects a crossover for the recovery to be interface-resistance dominated (small R) to either dilute-phase-diffusion or dense-phase-mixing dominated (large R). In the latter case, the fluo-

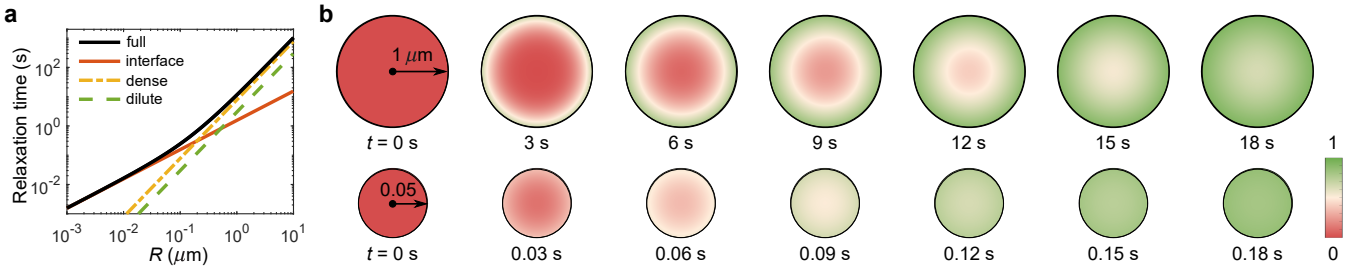

FIG. 4. **FRAP recovery patterns for large versus small droplets can be notably different for condensates with a sufficiently large interface resistance.** **a**, Relaxation time for modeled FRAP experiments as a function of droplet radius. The interface resistance is dominant for smaller droplets, while for larger droplets either dense- or dilute-phase diffusion can dominate. Parameters matched to the simulated A6B6 system: $c_{\rm den} = 7744\,\mu$M, $c_{\rm dil} = 50\,\mu$M, $D_{\rm den} = 0.013\,\mu{\rm m}^2/{\rm s}$, $D_{\rm dil} = 17\,\mu{\rm m}^2/{\rm s}$, and $\kappa = 0.2\,\mu$m/s. **b**, Time courses of fluorescence profiles for modeled FRAP experiments on droplets of radius $1\,\mu$m (top) and $0.05\,\mu$m (bottom); red is fully bleached, green is fully recovered.

rescence profile during recovery will be notably different in large versus small droplets as shown in Fig. 4b – for large droplets progressive diffusion of fluorescence into the droplet will be apparent, whereas small droplets will recovery uniformly, as internal mixing is fast compared to exchange with the surroundings. Thus observation of such a cross-over in recovery pattern at some considerable droplet size R provides evidence for the presence of a large interface resistance, which can be followed up by more quantitative studies.

In what phase-separated systems might the bouncing effect be present? The essential requirement is that molecules in the dilute phase should not present "sticky" surfaces to the dense phase. Since these same molecules must be capable of sticking to each other to phase separate, the natural scenario is that these molecules self-collapse into a non-sticky conformation in the dilute phase. Such conformations could involve shielding of non-specifically interacting regions, e.g. burial of hydrophobic residues in the core of a protein, or, in the scenario explored here, could result from the formation of strong saturable, sticker-like bonds within the molecule. Examples of systems with strong enough bonds include SIM-SUMO [20] and nucleic acids with strong intramolecular base-pairing. While in the case of LAF-1 the origin of the implied large interface resistance remains an open question, the current study suggests at least one possible mechanism: LAF-1 proteins in the dilute phase may adopt a conformation which is unlikely to stick to proteins in the dense phase, leading to frequent bouncing of incident LAF-1.

Biologically, the bouncing effect may also influence the coarsening of condensates. The same interface resistance that governs exchange between phases at equilibrium will control the flux of material from the dilute phase to the dense phase during coarsening. As many condensates dissolve and reform every cell cycle (or as needed) we anticipate that the bouncing effect may constitute an additional means of regulating condensate dynamics. Indeed, a recent theoretical study [21] of coarsening via mergers of small polymer clusters found anomalously slow dynamics due to exhaustion of binding sites, paralleling the single-polymer bouncing effect explored here.

III. ACKNOWLEDGMENTS

This work was supported in part by the National Science Foundation, through the Center for the Physics of Biological Function (PHY-1734030), NIH Grants R01 GM140032, U01 DA040601, the Howard Hughes Medical Institute, and the Air Force Office of Scientific Research (FA9550-20-1-0241 to CPB).

[1] Y. Shin and C. P. Brangwynne, Science **357**, eaaf4382 (2017).
[2] S. F. Banani, H. O. Lee, A. A. Hyman, and M. K. Rosen, Nat. Rev. Mol. Cell Biol. **18**, 285 (2017).
[3] S. An, R. Kumar, E. D. Sheets, and S. J. Benkovic, Science **320**, 103 (2008).
[4] X. Su, J. A. Ditlev, E. Hui, W. Xing, S. Banjade, J. Okrut, D. S. King, J. Taunton, M. K. Rosen, and R. D. Vale, Science **352**, 595 (2016).
[5] B. R. Sabari, A. Dall'Agnese, A. Boija, I. A. Klein, E. L. Coffey, K. Shrinivas, B. J. Abraham, N. M. Hannett, A. V. Zamudio, J. C. Manteiga, *et al.*, Science **361**, eaar3958 (2018).
[6] N. Formicola, J. Vijayakumar, and F. Besse, Traffic **20**, 639 (2019).
[7] R.-W. Yao, G. Xu, Y. Wang, L. Shan, P.-F. Luan, Y. Wang, M. Wu, L.-Z. Yang, Y.-H. Xing, L. Yang, *et al.*, Molecular Cell **76**, 767 (2019).

[8] N. O. Taylor, M.-T. Wei, H. A. Stone, and C. P. Brangwynne, Biophysical Journal **117**, 1285 (2019).

[9] E. S. F. Rosenzweig, B. Xu, L. K. Cuellar, A. Martinez-Sanchez, M. Schaffer, M. Strauss, H. N. Cartwright, P. Ronceray, J. M. Plitzko, F. Förster, *et al.*, Cell **171**, 148 (2017).

[10] S. Bo, L. Hubatsch, J. Bauermann, C. A. Weber, and F. Jülicher, Physical Review Research **3**, 043150 (2021).

[11] L. Hubatsch, L. M. Jawerth, C. Love, J. Bauermann, T. D. Tang, S. Bo, A. A. Hyman, and C. A. Weber, eLife **10**, e68620 (2021).

[12] J.-M. Choi, A. S. Holehouse, and R. V. Pappu, Annu. Rev. Biophys. **49** (2020).

[13] A. N. Semenov and M. Rubinstein, Macromolecules **31**, 1373 (1998).

[14] K. Kremer and G. S. Grest, J. Chem. Phys. **92**, 5057 (1990).

[15] LAMMPS Molecular Dynamics Simulator. Available from https://lammps.sandia.gov/.

[16] S. Plimpton, J. Comput. Phys. **117**, 1 (1995).

[17] B. G. Weiner, A. G. Pyo, Y. Meir, and N. S. Wingreen, PLoS Computational Biology **17**, e1009748 (2021).

[18] J. Brassinne, A. Cadix, J. Wilson, and E. Van Ruymbeke, Journal of Rheology **61**, 1123 (2017).

[19] P. Ronceray, Y. Zhang, X. Liu, and N. S. Wingreen, Physical Review Letters **128**, 038102 (2022).

[20] S. F. Banani, A. M. Rice, W. B. Peeples, Y. Lin, S. Jain, R. Parker, and M. K. Rosen, Cell **166**, 651 (2016).

[21] S. Ranganathan and E. I. Shakhnovich, eLife **9**, e56159 (2020).